The development of spatiotemporal dynamics of oscillatory activity in hiPSC-derived cortical tissue

Austin Hutton

Department of Cognitive Science, University of California San Diego

Honors Thesis Program

Advised by Dr. Bradley Voytek, Dr. Christian Cazares

June 13, 2025

The development of spatiotemporal dynamics of oscillatory activity in hiPSC-derived cortical tissue

Abstract

Coordinated neuronal activity is a characteristic and emergent feature in brain recordings. Human induced pluripotent stem cell (hiPSC) cultures offer a promising platform to identify the molecular and neural circuit origins of coordinated activity patterns, with unprecedented spatiotemporal resolution in human neural tissue, during pre-birth stages that are otherwise difficult to study during fetal cortex development. A growing body of work using human brain recordings has identified traveling waves, which are spatiotemporally organized patterns of neural activity, as one possible mechanism through which distant or distributed brain regions coordinate computational processes to facilitate cognition. However, it remains unclear how such structured dynamics emerge during early development, and whether they can be modeled in simplified, yet biologically representative, human-derived in vitro systems. In this study, we used hiPSC-derived cortical cultures expressing GABAergic, glutamatergic, and astrocytic molecular markers to investigate the spatiotemporal developmental trajectory of spontaneous and synchronized network activity. Cultures (n = 1,446) were plated and grown on microelectrode arrays (MEAs) to record spiking activity within ~300-second windows throughout 2 to 11 weeks post-plating. Preliminary analyses revealed a progressive increase in both spiking and bursting frequency during the first 7 weeks of development. Notably, individual cultures diverged into one of two distinct developmental profiles: either increasing burst frequency or increasing burst duration over time. These early trends suggest heterogeneous but organized modes of network maturation and provide a foundation for investigating the emergence of more structured dynamics. Ongoing analyses aim to quantify oscillatory (periodic), as well as broadband (aperiodic), spectral features, as well as the spatial propagation of these features to characterize how and when traveling waves and other meso-scale activity patterns emerge in the development of hiPSC cortical cultures. This work introduces a high-throughput, tractable system for studying the developmental basis of neural circuit organization that can be leverage to understand divergence from neurotypical development in cultures derived from patients affected by neurodevelopmental disorders.

Keywords: traveling waves, oscillations, human induced pluripotent stem cell, neurodevelopment

I. Introduction

Across cognitive functions, perceptual states, and levels of consciousness, temporally coordinated neural activity is essential for enabling organization in what would otherwise be a chaotic exchange among the brain's 80 billion neurons. Coordination at this scale can take different forms, be it in the brief but nearly simultaneous activation of a population leading to what is known as a population/network burst, or in the more sustained and recurrent rise and fall of a population's activity known as a neural oscillation. These temporally organized phenomena provide a mechanism through which neural populations represent and transmit complex

information, and have been fundamentally linked with cognition and behavior in both healthy and diseased brain activity (Buzsaki et al., 2004; Kim et al., 2019; Wang, 2010; Xie et al., 2024). Synchronized activity like neural oscillations are also thought to play an essential role in early cortical development by guiding circuit formation, synaptic refinement, and the emergence of functional connectivity (Khazipov & Luhmann, 2006; Gireesh & Plenz, 2008; Ben-Ari, 2002). While rhythmic oscillations across brain regions have a rich history of exploration in neuroscience studies, only relatively recently have the spatial characteristics of these phenomena garnered attention.

Traveling Waves. Traditionally, neural oscillations have been studied under the assumption of synchronized phases that are temporally anchored across participating populations. However, recent studies examining the full spatiotemporal structure of rhythmic activity have revealed that this synchronization can be more dynamic than rigid, involving continuously shifting phase offsets across spatially distributed neural populations—a phenomenon now referred to as *traveling waves* (Muller et al., 2018). Like oscillations, these traveling waves have also been functionally linked to different cognitive processes like working memory, visual processing, and reward representation, in both cortical and subcortical brain regions (Bhattacharya et al., 2022; Sreekumar et al. 2020; Davis et al., 2020; Zabeh et al., 2023). However, unlike oscillations, the physiological mechanisms that give rise to traveling waves remain largely unknown. One proposed theory suggests that they are an emergent property of axonal conduction delays in topographically organized networks, and may even spontaneously manifest during a range of asynchronous states of activity. (Davis et al., 2021). Studies have also shown that traveling waves exhibit substantial variability in their propagation direction, speed, and spatial form, with observed patterns including planar, spiral, and concentric geometries, each associated with distinct functional roles (Muller et al., 2018; Das et al., 2024; Xu et al., 2023). Despite growing interest in the mechanistic and functional origins of traveling waves, studies are limited in their ability to interrogate the developmental trajectories of such electrophysiological activity in vivo. As a result, the question of how traveling waves emerge and evolve within early-developing neural circuits remains unresolved.

Human Induced Pluripotent Stem Cells. The inaccessibility of human neural tissue during the earliest stages of neurodevelopment has driven the search for valid *in vitro* models, leading to the rise of human induced pluripotent stem cells (hiPSCs) as a promising platform for studying the electrophysiological characteristics of early neural circuit formation. These human-derived cell cultures are developed through the reprogramming of differentiated fibroblasts (though more accessible donor cell types are now also used) into pluripotent stem cells, which are then differentiated into neural progenitor cells (Shi et al., 2012). In the appropriate culture conditions, neural progenitor cells can generate a variety of neuronal and glia subtypes, including glutamatergic, GABAergic, dopaminergic, and astrocytic cells (Pelkonen et al., 2021). Importantly, these neural cultures retain their electrophysiological functioning and, depending on the cell types and relative proportions, can show a variety of spontaneous activity (Cerina et al., 2023). Additionally, technological advancements in multi-electrode array (MEA) devices have

enabled the high spatial and temporal resolution recording of hiPSC culture activity, without the need to disturb or compromise the structure or developmental trajectory of the culture. As the neural circuits in these cultures mature, synchronous and asynchronous patterns of activity emerge that, to a certain extent, recapitulate electrophysiological patterns observed in vivo (Kuijlars et al., 2016; Doorn et al., 2024), making hiPSC-derived neural tissue a promising avenue for investigating both neurodevelopment and disease pathology.

The Present Study. Despite an increasing number of recent studies exploring the electrophysiological properties of hiPSC-derived cortical tissue, the author of this paper knows of no published work investigating the emergence or evolution of traveling waves in these models. Because the underlying mechanisms of traveling waves remain mysterious, the simplified, highly controlled, and high-throughput advantages of hiPSC cortical models may offer unique insights into the basic origins of traveling waves, and may also be useful for furthering our understanding of mechanisms involved in the shaping of early development neural circuits. In light of this, the present study aims to leverage the advantages of in vitro models to resolve the spatiotemporal characteristics of spontaneous synchronous and asynchronous activity within hiPSC-derived cortical tissue. While this study is ongoing, preliminary results suggest distinct developmental trajectories for spiking and network burst activity in these cultures, which lay the foundation for future exploration of the emergence and possibly maturation of traveling waves in a novel experimental context.

II. Materials

Data Overview. Through collaboration with the lab of Dr. Ann Bang at the Sanford Consortium, we received spike timing data from hiPSC cultures generated with approximately 60% glutamatergic, 12% GABAergic, 12% dopaminergic, and 10% astrocyte cell types. Immunostaining was performed to confirm cell type proportions, in addition to the presence of both pre- and postsynaptic protein markers to confirm functional synaptic connectivity within the networks. Cultures were grown on Axion Biosystems 48-well MEA plates (each well's MEA was a 4x4 grid of electrodes totaling 16 channels for recording) of which there were 8 plates (384 unique wells) recorded during weeks 2 to 11 after plating. MEA recordings were performed at weekly intervals for ~300 seconds with a sample rate of 12.5 kHz. Not every plate was recorded at every weekly timepoint, but in total there were 2,016 well recordings across the 10 timepoints (see Figure 3 for sample sizes at each time point).

Exclusion Criteria. For the purposes of analyzing spatiotemporal dynamics, a custom exclusion criterion was implemented to serve both as a quality control measure and to ensure that wells included in the analysis were at least minimally active over an area of the MEA sufficient to allow spatial patterns to be observed. At any timepoint, if a well did not exceed a mean spike frequency greater than 5 Hz or the MEA did not show more than 4 channels (25%) with any amount of spiking activity (>1 spike during recording), that recording was excluded from the overall analysis. Post exclusion, there were a total of 1,446 well recordings across the 10 timepoints.

Computational Tools. Spike timestamp data was extracted from data structures using MATLAB, with careful consideration for ensuring that spatial relationships among MEA channels were preserved during formatting. All analyses and data visualizations were performed in Python using custom scripts, with the exception of the MaxInterval algorithm for detecting single-channel bursts, which was adapted from Kartik Pradeepan's open-source code (Pradeepan, 2022). Additional python libraries incorporated in the analysis pipeline include numpy and pandas (data handling), scipy and statsmodels (computational operations and statistical analyses), and matplotlib and seaborn (data visualization).

III. Methods

Spiking Activity. Spike frequency was calculated by summing the total number of spike occurrences across all 16 channels in a given well and dividing by the length of the recording (seconds). A stacked histogram of spike frequency distributions at each timepoint was generated to assess data quality. Mean spike frequencies were calculated for each individual timepoint and visualized to identify any preliminary developmental trends.

Single-Channel Bursts. Burst detection on individual electrodes was performed using the MaxInterval algorithm, a rule-based method that identifies bursts by evaluating inter-spike intervals (ISIs) within a spike train. A single-channel burst was defined as a contiguous series of spikes meeting all of the following criteria which were adapted from the work of Cotterill et al. (2016) comparing approaches and parameters for robust burst detection: maximum ISI to initiate burst = 0.2 seconds, maximum ISI to end burst = 0.3 seconds, minimum inter-burst interval = 0.2 seconds, minimum burst duration = 10 milliseconds, minimum spikes per burst = 5. Each spike train (from each electrode in each well) was passed through this algorithm to generate a list of burst events, which were used to create per-well dictionaries of burst start and end times for each channel (Figure 1B).

Network Bursts. Network bursts were defined as periods of widespread, overlapping bursting activity across electrodes within a single well. To identify episodes of synchronized activity at the network level across each well, a custom method was implemented to detect network bursts based on the temporal overlap of single-channel bursts across the MEA. For each well, the number of active electrodes (channels that detected least one spike during the recording) were stored and a binary burst matrix was created with dimensions [4 × 4 × number of samples], where each entry indicated whether a given channel was engaged in a burst at each sample index during the recording. This matrix was summed across spatial dimensions to yield a time series representing the number of electrodes simultaneously bursting at each sample. The initiation of a network burst was defined as any sample index for which at least 50% of total active electrodes for a well were bursting, and was terminated when this number dropped below 20%. Bursts occurring within 1 second of each other were merged, after which any burst shorter than 0.5 seconds in duration was discarded (Figure 1A). For each detected network burst, the start and end sample indices were stored in dictionaries, and well-level summary features were computed,

including: network burst count (total number of detected network bursts), network burst frequency (network burst count divided by total recording duration), and mean network burst duration.

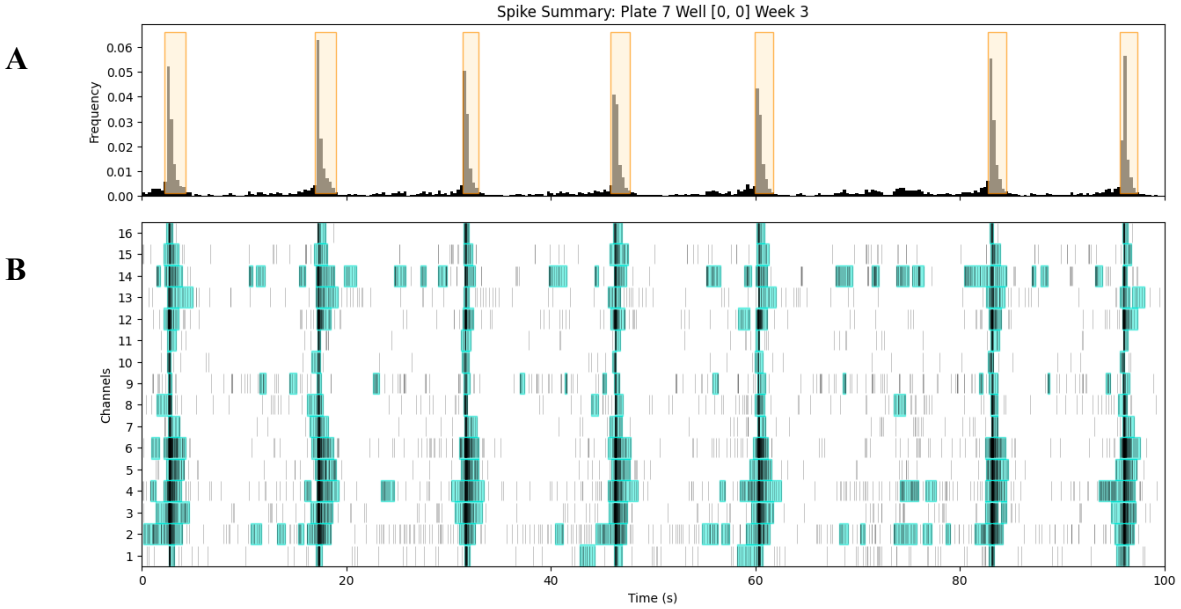

Figure 1. Example structure of spiking data for a single well during part of a recording with burst detection algorithm output overlayed. (A) Network Activity Histogram across time showing regular transient spiking events resulting from synchronized activity across channels. Network histograms are density-scaled, and reflect aggregated spikes across all 16 MEA channels. Orange windows are detected network burst events. (B) Raster plot of recorded spikes from all 16 channels of MEA across time. Blue windows are detected single channel burst events.

Statistical Modeling. To assess developmental changes in neural activity features (e.g., spike frequency, network burst frequency, and network burst duration), linear mixed-effects (LME) models were implemented using the statsmodels package in Python. LME models were selected due to their suitability for handling imbalanced and incomplete sampling across timepoints (not all plates were recorded at every week, and wells meeting the exclusion criterion were discarded from analysis, resulting in variable and discontinuous samples across recording weeks). These models accounted for repeated measurements from the same wells and controlled for non-independence introduced by the experimental design. For each model, the developmental timepoint (weeks 2–11) was treated as a fixed effect, and random intercepts were specified for each well using a combined plate-well identifier (Plate_Well_ID). The general model structure was:

$$\text{Feature} \sim \text{Timepoint} + (1 \mid \text{Plate\_Well\_ID})$$

To characterize how developmental trends evolved over time, this model was fit across a series of increasing time windows (e.g., weeks 2–5, 2–6, …, 2–11). This strategy enabled evaluation of

whether early trends stabilized, intensified, or reversed as additional later timepoints were included, providing finer-grained insight into the trajectory of network activity maturation.

IV. Results

Spiking Analysis. For the 1,446 recordings passing the exclusion criteria across the 10 week period starting with week 2, spike frequency histograms showed visibly increasing distributional variability from weeks 2 to 6, with a breakdown in unimodality after week 6 (Figure 2). Mean and median spike frequency for each time point increased steadily from week 2 to week 8, with a notable upward shift in week 3 (Figure 3). The linear mixed effects model reflected this trend, and showed that, relative to week 2, spike frequency was significantly higher at all subsequent timepoints, with the largest fixed effect observed at week 8 ($\beta = 4.01$, SE = 0.33, $p < 0.001$; Figure 4; Table 1). Coefficients remained significant through week 11, though a downward trend was observed after the peak.

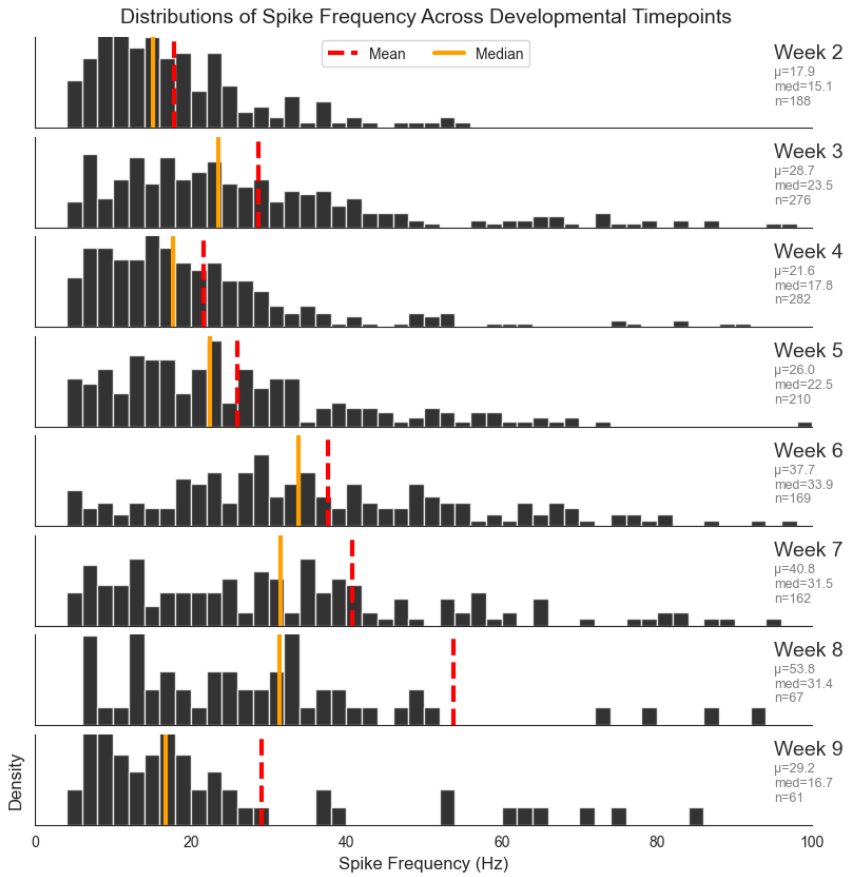

Figure 2. Spike frequency (average incidence of spiking in hertz) distributions for all wells from week 2 to 9. Each panel includes the sample size (n), mean (μ, red dashed line), and median (med, yellow line) spike frequency for that timepoint. Over development, the distributions become broader and more variable, particularly between weeks 2 and 6, after which sample size declines and variability appears to taper. The shift from unimodal to right-skewed distributions shows increasing heterogeneity in spiking activity across wells as networks mature.

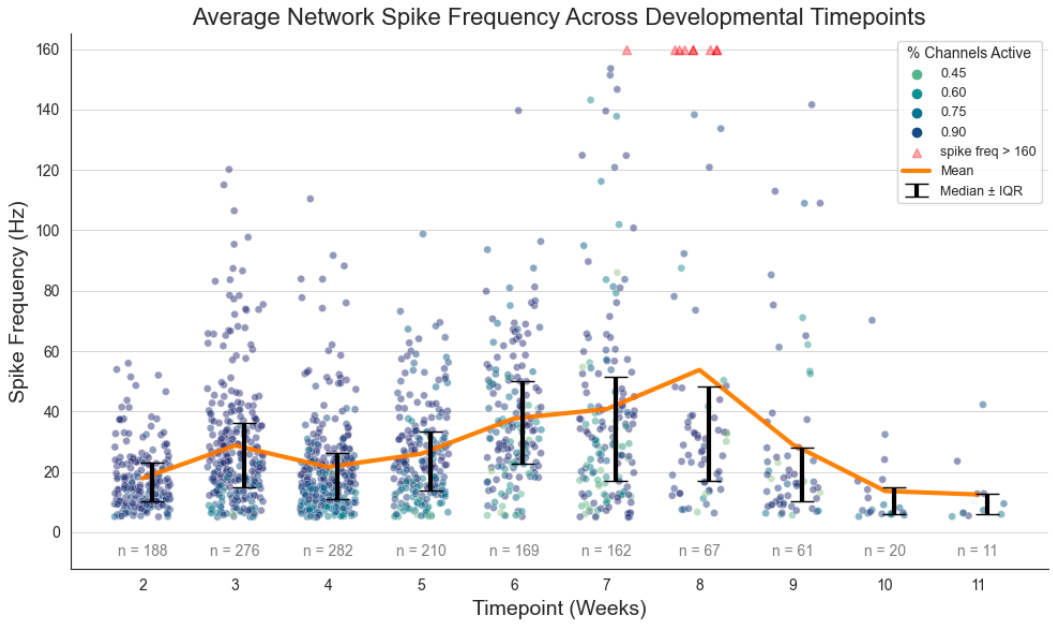

Figure 3. Average spike frequency across developmental timepoints. Each point represents the mean spike frequency (Hz) of a single well, color-coded by the proportion of active electrodes (% channels with ≥1 spike). Orange line indicates the population mean at each week, while black bars represent the median ± interquartile range (IQR). Triangular markers highlight extreme outliers (>160 Hz). Sample sizes (n) are shown along the x-axis. Spike frequency generally increased from weeks 2 to 8 before declining, suggesting an early developmental rise in excitability followed by a stabilization or dropout of high-activity wells.

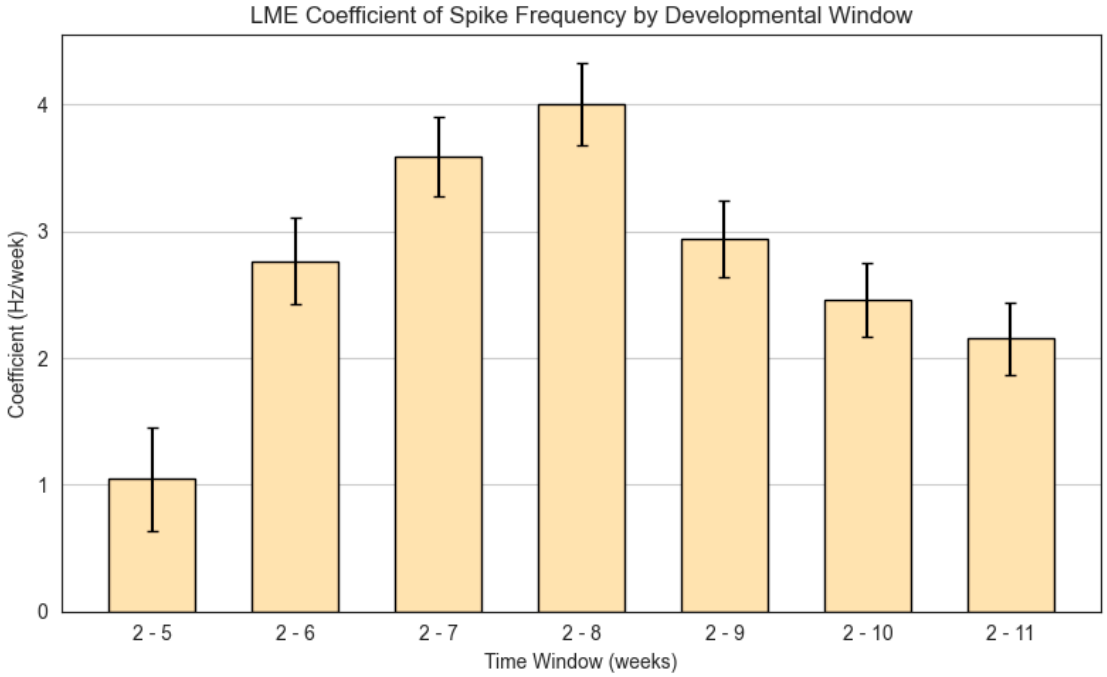

Figure 4. Linear mixed-effects model coefficients for spike frequency across increasing developmental windows. Each bar represents the estimated fixed-effect coefficient (Hz/week) of timepoint on spike frequency within the specified developmental window. Error bars indicate standard error of the estimate. The slope increased from early windows (2–5) to a peak at 2–8, then declined in later windows.

weeks	coef	se	95% ci_lower	95% ci_upper	p	n_obs
2-5	1.044	0.409	0.243	1.845	0.011	956
2-6	2.764	0.343	2.092	3.435	0.000	1125
2-7	3.592	0.312	2.981	4.203	0.000	1287
2-8	4.005	0.327	3.364	4.647	0.000	1354
2-9	2.937	0.301	2.346	3.528	0.000	1415
2-10	2.458	0.291	1.888	3.027	0.000	1435
2-11	2.153	0.284	1.597	2.709	0.000	1446

Table 1. Statistical estimates from the linear mixed-effects models shown in Figure 4. Coefficients represent the estimated fixed-effect of developmental timepoint (Hz/week) on spike frequency within each window. Standard errors (SE), 95% confidence intervals, p-values, and sample sizes (n_obs) are reported for each model.

Network Burst Analysis. Network burst frequency and duration were calculated for each well across the 10-week recording period. Burst frequency increased from week 2, peaked at week 6, and declined through week 11 (Figure 5A). Burst duration increased more gradually and peaked later, at week 8, before declining in the final timepoints (Figure 5B).

To evaluate these developmental trends statistically, linear mixed-effects models were fit over increasing developmental time windows from weeks 2 to 5 through 2 to 11. The model for burst frequency yielded a peak slope in the 2–8 week window ($\beta = 0.00445$ Hz/week, SE = 0.00055, $p < 0.001$; Table 2; Figure 6A), consistent with the observed trajectory. The model for burst duration showed the strongest positive slope in the 2–7 week window ($\beta = 0.95$ s/week, SE = 0.069, $p < 5.0e{-}43$), after which the effect size declined (Table 2; Figure 6B).

V. Discussion

The present study characterized the basic developmental progression of spontaneous spiking and bursting activity in hiPSC-derived cortical cultures over a 10-week period. Analyses revealed nonlinear developmental trajectories in both spike frequency and network-level burst features, offering insight into the maturation of coordinated activity in a simplified in vitro model of human cortical tissue. Spiking activity in these cultures increased steadily during the early stages of development, with a clear peak in network maturation occurring around weeks 7 to 8. This pattern suggests ongoing structural or synaptic changes that support greater excitability and signal propagation across the network. Parallel increases in coordinated activity like network burst frequency and duration further suggest that these developing networks undergo circuit-level refinements that promote coordinated population dynamics. Because burst frequency and duration are inversely related (in a finite time window, higher frequency events must be shorter in duration), the data points to heterogeneous modes of development, wherein some networks begin sustaining longer network burst events and others produce increasingly shorter but more frequent bursts

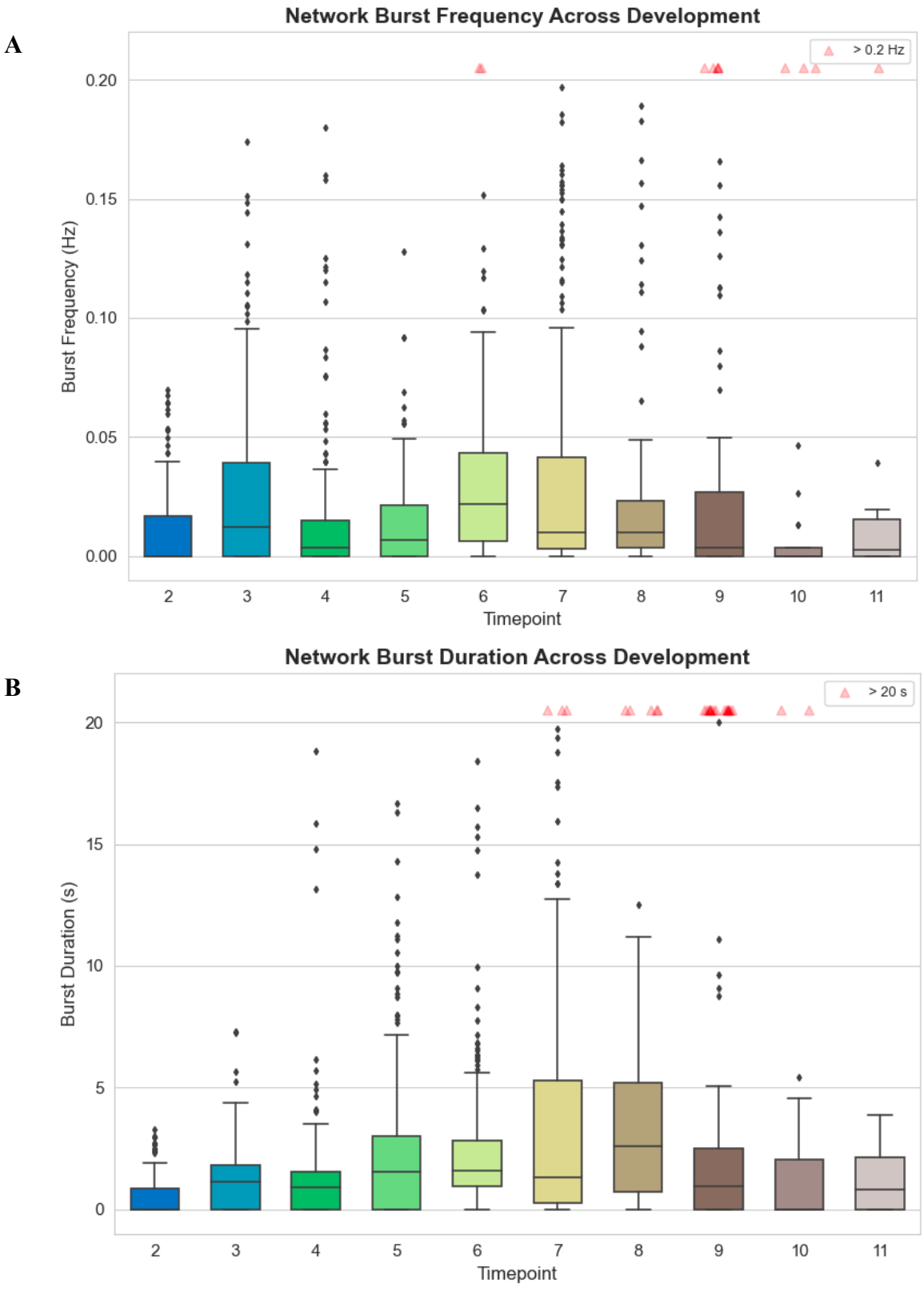

Figure 5. Distribution of (A) network burst frequency and (B) duration across developmental timepoints. Boxplots show median, interquartile range, and outliers for each week from 2 to 11. Pink triangles indicate extreme outliers with burst frequency greater than 0.2 Hz.

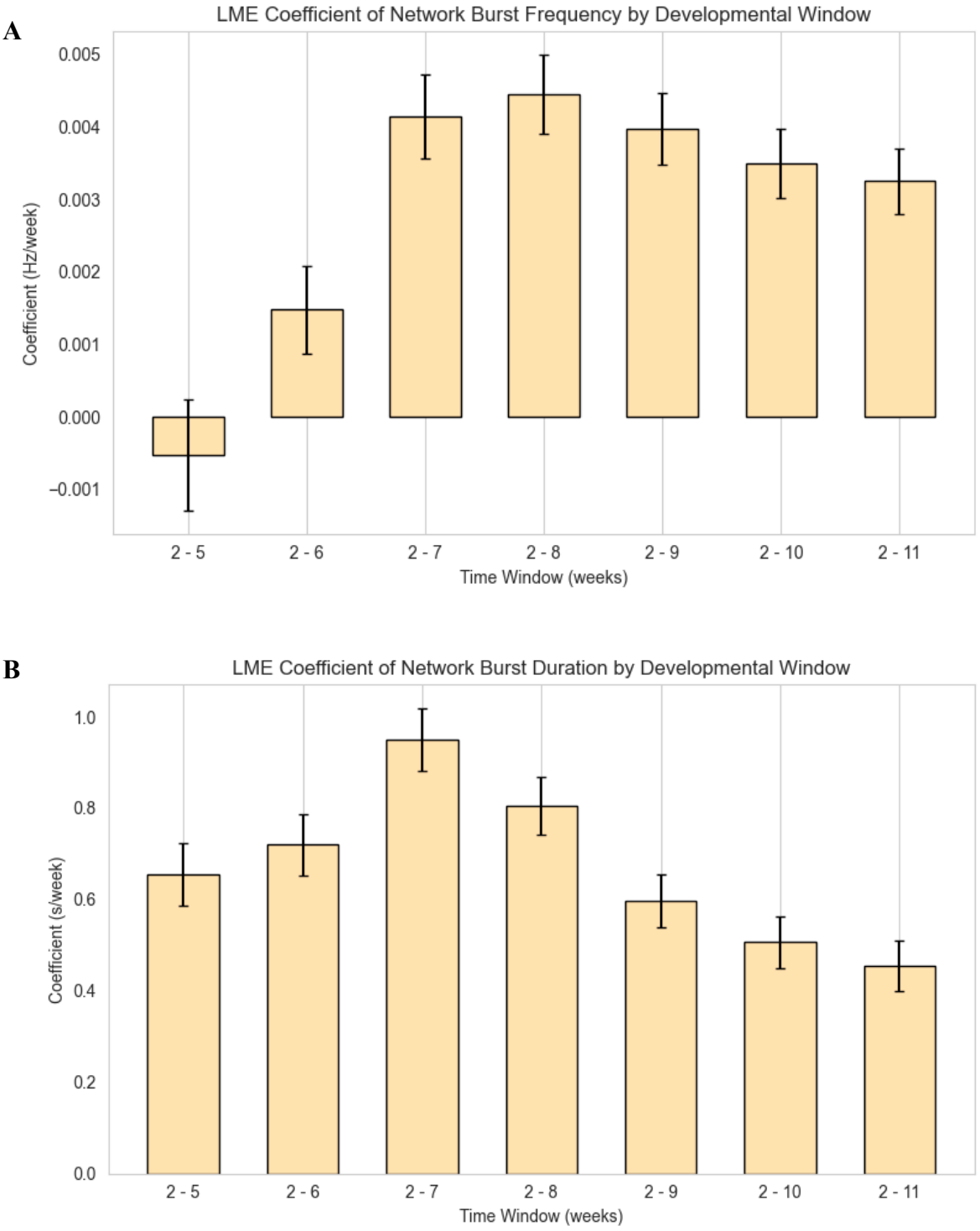

Figure 6. Linear mixed-effects model coefficients for (A) network burst frequency and (B) network burst duration across increasing developmental windows. Each bar reflects the estimated fixed-effect coefficient of time (in Hz/week for frequency, s/week for duration) on the corresponding burst feature within the specified time window. Error bars indicate standard error of the estimate. Developmental slopes peaked in the 2–8 window for burst frequency and the 2–7 window for burst duration, followed by declines, indicating temporally bounded phases of maturation.

weeks	coef	se	95% ci_lower	95% ci_upper	p	n_obs
Network Burst Frequency						
2-5	-0.001	0.001	-0.002	0.001	0.497	956
2-6	0.001	0.001	0.000	0.003	0.014	1125
2-7	0.004	0.001	0.003	0.005	0.000	1287
2-8	0.004	0.001	0.003	0.006	0.000	1354
2-9	0.004	0.000	0.003	0.005	0.000	1415
2-10	0.003	0.000	0.003	0.004	0.000	1435
2-11	0.003	0.000	0.002	0.004	0.000	1446
Network Burst Duration						
2-5	0.655	0.068	0.522	0.788	0.000	956
2-6	0.720	0.067	0.588	0.852	0.000	1125
2-7	0.950	0.069	0.815	1.085	0.000	1287
2-8	0.805	0.064	0.680	0.929	0.000	1354
2-9	0.597	0.058	0.483	0.711	0.000	1415
2-10	0.507	0.056	0.396	0.617	0.000	1435
2-11	0.456	0.055	0.348	0.564	0.000	1446

Table 2. Statistical estimates from the linear mixed-effects models shown in Figure 6. Coefficients represent the estimated fixed-effect of developmental timepoint (Hz/week) on spike frequency within each window. Standard errors (SE), 95% confidence intervals, p-values, and sample sizes (n_obs) are reported for each model.

Establishing the cellular and molecular mechanisms enabling these electrophysiological trends is outside the scope of this project, but it is possible that the observed developmental changes are facilitated by processes related to synaptic plasticity, such as long-term potentiation and depression. These mechanisms may differentially shape synaptic strength and connectivity depending on the types of neurons involved, the specific circuits they form, and the patterns of early activity within the network. These trends may also reflect differences in the balance of excitation and inhibition in the network, both over the long-term development of the culture and during transient network burst events.

Important limitations should be considered when interpreting these results, taking into account both the experimental constraints and analysis decisions. First, while hiPSCs can serve as a useful model for in vivo human cortical tissue, there remain several differences that could limit the generalizability of these findings. Structurally, hiPSC cortical cultures are simplified neural systems that lack layered, three-dimensional architecture as well as long-range projections to distant, diverse cell populations. Additionally, cortical cultures in this experiment are without

external input, and thus do not reflect in vivo systems that might receive stimulation from sensory or subcortical sources. Second, limitations to the analysis are introduced in several stages, including the exclusion of a subset of inactive cell cultures and the somewhat arbitrary burst detection parameters. While this was considered necessary for resolving later spatiotemporal characteristics (and robustness of future results will involve testing a variety parameter values), only including cultures surpassing a minimum threshold of activity for a minimum number of MEA channels could be overrepresenting more excitable or regularly spiking networks, or exclude sufficiently active networks that simply do not produce spikes close enough to a majority of the recording electrodes. Finally, the present analyses were only focused on simplified metrics of hiPSC activity (spike frequency, and network burst frequency and duration), which, while useful for describing broad developmental trends, could be missing potentially richer dynamics. Nonetheless, these preliminary characterizations lay a necessary foundation for future work exploring more complex manifestations of coordinated network activity.

Building on these preliminary developmental findings, continued efforts on this project will aim to characterize and compare spectral and spatial features of network activity in these same hiPSC cultures, looking specifically to map changes in oscillatory activity, including its spatial organization, onto developmental trends observed in the present analyses. Ultimately, we hope to identify whether traveling waves emerge in hiPSC cortical cultures, and determine which basic features of development they coincide with in order to start understanding how different scales of spatiotemporal coordination emerge in the human cortex. Identifying the developmental properties of traveling waves in vitro could provide valuable insight into the circuit-level mechanisms that sculpt cortical networks to support early cognitive function, and may also serve as a comparative benchmark for investigating deviations from typical neurodevelopment in patient-derived cell lines.

Acknowledgments. I would like to thank my advisors to this project, Dr. Bradley Voytek and Dr. Christian Cazares, for their endless contributions to this work, from inspiring its genesis to recommending analytical approaches and offering insightful interpretations of the findings. I have so much gratitude for their time and consideration, and a deep appreciation for their compassionate approach to undergraduate mentorship. Thank you to Dr. Ann Bang, Dr. Deborah Pre, and Alexander Wooten for their collaboration, allowing me to work with the data they worked so hard to collect, and for offering insight into the experimental inner workings of this data set. Many thanks are also extended to my faculty mentors and colleagues in the Cognitive Science Department for their continual support and their principled, constructive feedback. Additionally, I would like to acknowledge my mentors in the STARTneuro Program, without whom I would never have believed a career in research was possible. Thank you to the NIH BP-ENDURE initiative for supporting diverse undergraduates and programs making neuroscience research more accessible. And finally, thanks to my friends and family for encouraging me to follow my passions.

References

Ben-Ari, Y. (2002). Excitatory actions of GABA during development: The nature of the nurture. *Nature Reviews Neuroscience*, *3*(9), 728–739. https://doi.org/10.1038/nrn920

Bhattacharya, S., Brincat, S. L., Lundqvist, M., & Miller, E. K. (2022). Traveling waves in the prefrontal cortex during working memory. *PLoS Computational Biology*, *18*(1), e1009827. https://doi.org/10.1371/journal.pcbi.1009827

Buzsaki, G., & Draguhn, A. (2004). Neuronal oscillations in cortical networks. *Science*, *304*(5679), 1926–1929. https://doi.org/10.1126/science.1099745

Cerina, M., Piastra, M. C., & Frega, M. (2023). The potential of in vitro neuronal networks cultured on micro electrode arrays for biomedical research. *Progress in Biomedical Engineering*, *5*(3), 032002–032002. https://doi.org/10.1088/2516-1091/acce12

Cotterill, E., Charlesworth, P., Thomas, C. W., Paulsen, O., & Stephen John Eglen. (2016). A comparison of computational methods for detecting bursts in neuronal spike trains and their application to human stem cell-derived neuronal networks. *Journal of Neurophysiology*, *116*(2), 306–321. https://doi.org/10.1152/jn.00093.2016

Das, A., Zabeh, E., Ermentrout, B., & Jacobs, J. (2024). Planar, spiral, and concentric traveling waves distinguish cognitive states in human memory. *BioRxiv*. https://doi.org/10.1101/2024.01.26.577456

Davis, Z. W., Benigno, G., Fletterman, C., Desbordes, T., Steward, C., Sejnowski, T. J., Reynolds, J. H., & Muller, L. (2021). Spontaneous traveling waves naturally emerge from horizontal fiber time delays and travel through locally asynchronous-irregular states. *Nature Communications*, *12*(1). https://doi.org/10.1038/s41467-021-26175-1

Davis, Z. W., Muller, L., Martinez-Trujillo, J., Sejnowski, T., & Reynolds, J. H. (2020). Spontaneous travelling cortical waves gate perception in behaving primates. *Nature*, *587*(7834), 432–436. https://doi.org/10.1038/s41586-020-2802-y

Doorn, N., Voogd, E., Levers, M. R., van Putten, M., & Frega, M. (2024). Breaking the burst: Unveiling mechanisms behind fragmented network bursts in patient-derived neurons. *Stem Cell Reports*, *9*(11). https://doi.org/10.1016/j.stemcr.2024.09.001

Gireesh, E. D., & Plenz, D. (2008). Neuronal avalanches organize as nested theta- and beta/gamma-oscillations during development of cortical layer 2/3. *Proceedings of the National Academy of Sciences*, *105*(21), 7576–7581. https://doi.org/10.1073/pnas.0800537105

Khazipov, R., & Luhmann, H. J. (2006). Early patterns of electrical activity in the developing cerebral cortex of humans and rodents. *Trends in Neurosciences*, *29*(7), 414–418. https://doi.org/10.1016/j.tins.2006.05.007

Kim, J. H., Lee, H. J., Choi, W., & Lee, K. J. (2019). Encoding information into autonomously bursting neural network with pairs of time-delayed pulses. *Scientific Reports*, *9*(1). https://doi.org/10.1038/s41598-018-37915-7

Kuijlaars, J., Oyelami, T., Diels, A., Rohrbacher, J., Versweyveld, S., Meneghello, G., Tuefferd, M., Verstraelen, P., Detrez, J. R., Verschuuren, M., De Vos, W. H., Meert, T., Peeters, P. J., Cik, M., Nuydens, R., Brône, B., & Verheyen, A. (2016). Sustained synchronized neuronal network activity in a human astrocyte co-culture system. *Scientific Reports*, *6*(1). https://doi.org/10.1038/srep36529

Muller, L., Chavane, F., Reynolds, J., & Sejnowski, T. J. (2018). Cortical travelling waves: Mechanisms and computational principles. *Nature Reviews Neuroscience*, *19*(5), 255–268. https://doi.org/10.1038/nrn.2018.20

Pelkonen, A., Pistono, C., Klecki, P., Gómez-Budia, M., Dougalis, A., Konttinen, H., Stanová, I., Fagerlund, I., Leinonen, V., Korhonen, P., & Malm, T. (2021). Functional characterization of human pluripotent stem cell-derived models of the brain with microelectrode arrays. *Cells*, *11*(1), 106–106. https://doi.org/10.3390/cells11010106

Pradeepan, K. (2022). *MaxInterval burst detection algorithm (python/matlab) | kartik pradeepan*. Kartikpradeepan.com. https://www.kartikpradeepan.com/projects/MaxInterval/

Shi, Y., Kirwan, P., & Livesey, F. J. (2012). Directed differentiation of human pluripotent stem cells to cerebral cortex neurons and neural networks. *Nature Protocols*, *7*(10), 1836–1846. https://doi.org/10.1038/nprot.2012.116

Sreekumar, V., Wittig, J. H., Chapeton, J. I., Inati, S. K., & Zaghloul, K. A. (2020). Low frequency traveling waves in the human cortex coordinate neural activity across spatial scales. *BioRxiv*. https://doi.org/10.1101/2020.03.04.977173

Wang, X.-J. (2010). Neurophysiological and computational principles of cortical rhythms in cognition. *Physiological Reviews*, *90*(3), 1195–1268. https://doi.org/10.1152/physrev.00035.2008

Xie, W., Wittig, J. H., Chapeton, J. I., El-Kalliny, M., Jackson, S. N., Inati, S. K., & Zaghloul, K. A. (2024). Neuronal sequences in population bursts encode information in human cortex. *Nature*, *635*(8040), 935–942. https://doi.org/10.1038/s41586-024-08075-8

Xu, Y., Long, X., Feng, J., & Gong, P. (2023). Interacting spiral wave patterns underlie complex brain dynamics and are related to cognitive processing. *Nat Hum Behaviour* **7**, 1196–1215. https://doi.org/10.1038/s41562-023-01626-5

Zabeh, E., Foley, N. C., Jacobs, J., & Gottlieb, J. P. (2023). Beta traveling waves in monkey frontal and parietal areas encode recent reward history. *Nature Communications*, *14*(1). https://doi.org/10.1038/s41467-023-41125-9